SI: Harnessing DFT and Machine Learning for Accurate Optical Gap Prediction in Conjugated Polymers

Bin Liu[1,2†], Yunrui Yan[1,2†], and Mingjie Liu[1,2*]

[1]Department of Chemistry, University of Florida, Gainesville, FL 32611, United States.

[2]Quantum Theory Project, University of Florida, Gainesville, FL 32611, United States.

[†]These authors contributed equally to this work.

[*]Corresponding author. E-mail: mingjieliu@ufl.edu

February 11, 2025

1 Note S1. RDKit Descriptor Selection

We applied the following steps to select features from 209 RDKit descriptors that are relevant to the target property (e.g., optical band gap E_{gap}^{exp}) and to remove redundant variables that are highly correlated with each other: (i) removal of descriptors with missing values, infinite values, and constant values; (ii) removal of descriptors with a pairwise Pearson correlation coefficient (P_{pair}) greater than or equal to 0.90; (iii) removal of descriptors with a Pearson correlation coefficient with respect to the optical band gap (P_{gap}) less than or equal to 0.05. We tested different combinations of P_{pair} and P_{gap} values with the XGBoost model for optical band gap prediction, with the performance metrics presented in Table S2. The list of 54 RDKit descriptors selected for predicting experimental optical gap is shown in Table S3.

2 Note S2. Model Training Strategy

We applied 10-fold cross validation (CV) method[1] to train the ML models as shown in Figure S3. First, the whole dataset of 1096 data points was randomly divided into 10 subsets. We used 9 subsets as the training set and 1 as the test set. This procedure was repeated 10 times by rotating each of the 10 subsets as the test set. The training data in each subset was further divided into training and validation by an extra 10-fold CV. For each test set in the 10-fold CV, the average value calculated from the extra 10-fold CV was used as the prediction value. The ML model accuracy

was determined by the average performance metrics (RMSE, MAE, R^2, r) of the 10-fold CV. The hyper-parameters can be found in Table S14.

3 Note S3. Model Performance Metrics

In this work, we applied four metrics to evaluate the effectiveness of ML models for predicting experimental optical gap, including coefficient of determination (R^2), Pearson correlation coefficient (r), Root mean square error (RMSE), and mean absolute error (MAE). The definitions of four metrics were shown as follows.

$$R^2 = 1 - \frac{\sum_{i=1}^{n}(y_i - x_i)^2}{\sum_{i=1}^{n}(\bar{y} - x_i)^2} \tag{1}$$

$$r = \frac{\sum_{i=1}^{n}(x_i - \bar{x})(y_i - \bar{y})}{\sqrt{\sum_{i=1}^{n}(x_i - \bar{x})^2}\sqrt{\sum_{i=1}^{n}(y_i - \bar{y})^2}} \tag{2}$$

$$RMSE = \sqrt{\frac{1}{n}\sum_{i=1}^{n}(y_i - x_i)^2} \tag{3}$$

$$MAE = \frac{1}{n}\sum_{i=1}^{n}|y_i - x_i| \tag{4}$$

in which x_i and y_i represent the experimental and predicted band gap values, and $\bar{x}$ and $\bar{y}$ represent the mean value of experimental and predicted values, respectively.

4 Note S4. Differences Among the Six Machine Learning Algorithms

In this section, we summarize the differences among six commonly used machine learning algorithms, highlighting their unique features and strengths for various tasks.

1. **XGBoost:** A gradient-boosted decision tree algorithm that uses regularization to prevent overfitting. It is highly efficient for structured data and includes hyperparameters like learning rate and tree depth.

2. **HGBR (Histogram-Based Gradient Boosting Regressor):** Similar to XGBoost but designed for faster computation by using histogram-based binning, particularly effective for large datasets.

3. **LGBM (Light Gradient Boosting Machine):** A boosting framework that splits trees leaf-wise instead of level-wise, leading to better accuracy for imbalanced datasets.

4. **GBR (Gradient Boosting Regressor):** A classic implementation of boosting for regression problems, which uses shallow trees to improve robustness against overfitting.

5. **AdaBoost:** Focuses on sequentially correcting errors by assigning higher weights to misclassified samples during training, making it sensitive to noise.

6. **RF (Random Forest):** A bagging-based ensemble learning method that builds multiple decision trees and averages their predictions, prioritizing robustness and reducing variance.

5 Note S5. Oligomer structure construction

Given the limited understanding of the correlation between the conjugation length of backbone chain and the electronic properties of CPs, we calculated the HOMO, LUMO, and gap values of four polymer structures with different repeating units (see Figure S4 and Table S4). Based on our tests, we have established following guidelines for constructing oligomer structures to effectively capture the electronic properties of CPs: First, the oligomer should comprise at least four aromatic blocks linked by C-C single bonds along the backbone chain. Second, the structure should consist of at least six aromatic rings. Commonly used aromatic rings include thiophene, furan, pyrrole, benzene, and their derivatives. These aromatic rings can combine to form larger aromatic units such as benzodithiophene (BDT), which consists of two thiophenes and one benzene. In addition, monomers containing over four aromatic blocks with over eight aromatic rings can be employed for DFT calculations as they already contain sufficient conjugation to mimic the properties of larger oligomer. In the case of BDT-T polymer, the monomer consists of two building blocks with four aromatic rings in total. Thus, the dimer structure, which contains four building blocks with eight aromatic rings along the backbone chain, meets the outlined criteria (see Table S4).

6 Note S6. Exchange-correlation functional test

The DFT-calculated HOMO-LUMO gaps are notably influenced by the choice of exchange-correlation (xc) functionals. A variety of xc functionals have been extensively applied to the study of organic molecules and CP materials systems for both ground and excited state electronic property calculations.[2–4] In this study, we investigated the correlations among four xc functionals for HOMO-LUMO gap calculations with oligomer structures: PBE at the GGA level, and the hybrid-GGA functionals B3LYP, ωB97XD, and CAM-B3LYP. Table S5 illustrates that all four functionals achieve Pearson correlation coefficients (r) above 0.96 among each other. Furthermore, linear fits between these functionals, detailed in Figure S5, yielded R^2 values ranging from 0.922 to 0.999. These results suggest that while different xc functionals produce varying absolute HOMO-LUMO gap values, their relative correlations remain strong. Thus, the four xc functionals demonstrate similar performance metrics in linear regression between DFT and experimental gaps, with ωB97XD showing slightly superior correlation, evidenced by higher R^2 and lower MAE values (see Table S6).

Additionally, we utilized the TDDFT method at the B3LYP level to calculate the lowest excited states (S1) for oligomers. As shown in Figure S6, TDDFT-calculated S1 state energies are highly correlated with DFT calculated HOMO-LUMO gaps with a R^2 value of 0.973. The performance metrics of linear regression for predicting optical gaps with S1 values were presented in Table S7.

Our results suggest that employing lower-level xc functionals for ground state electronic structure calculations is preferable for generating quantum chemical descriptors in machine learning model training, optimizing the balance between prediction accuracy and computational efficiency for high-throughput material screening.

7 Note S7. SHAP Analysis of Feature Importance

To compare the importance of individual features in predicting the optical band gap, SHAP (SHapley Additive exPlanations) analysis was performed for models trained with oligomer-derived DFT-calculated HOMO-LUMO gaps. The results (Figure S7) provide a clear comparison of the top five most important features for each model.

Across all machine learning models, DFT-calculated HOMO-LUMO gap emerges as the most influential feature, with its mean SHAP value substantially exceeding those of other descriptors. Meanwhile, RDKit descriptors such as `fr_C=O` and `VSA_EState2` are consistently among the top five impactful features, indicating that the structural information they provide effectively complements the electronic properties captured by the DFT-calculated gap. These findings highlight the strong predictive capability of the DFT-calculated HOMO-LUMO gap of oligomers in representing extended conjugation and electronic structure, while the inclusion of structural descriptors further refines model performance by capturing additional molecular variations.

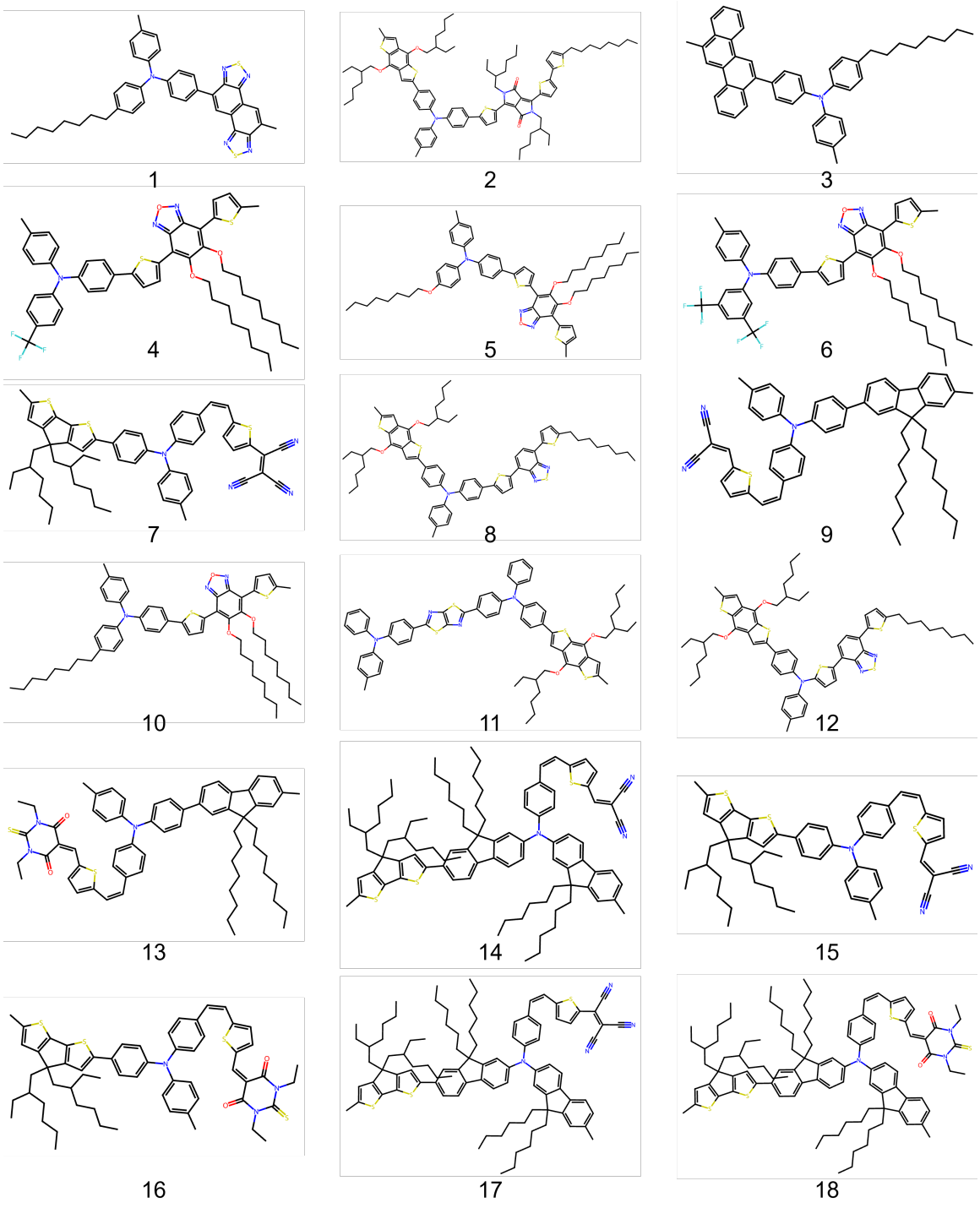

Figure S1: Chemical structures of 18 non-conjugated polymers containing sp3-hybridized N atom along backbone chain.

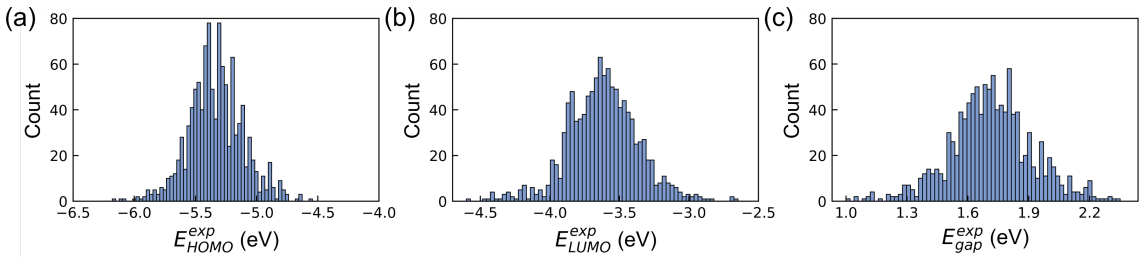

Figure S2: The distributions of the experimentally measured HOMO, LUMO, and optical band gap (E^{exp}_{gap}) values of the conjugated polymers in the dataset with 1096 data points. Unit: eV.

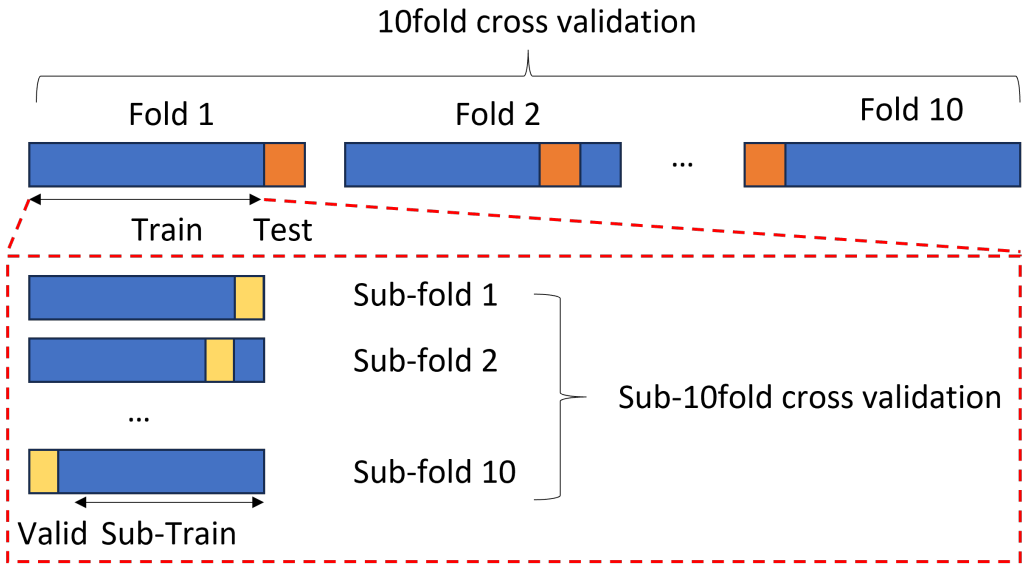

Figure S3: The model training process with 10-fold cross validation (CV) method. For each train set, an extra 10-fold CV was applied.

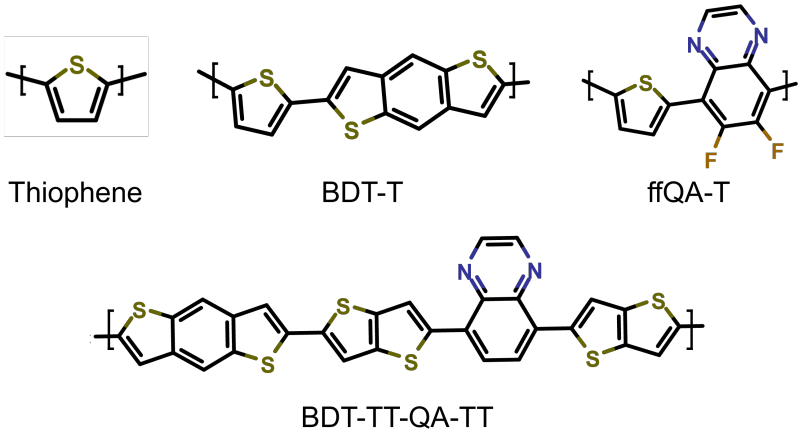

Figure S4: Chemical structures of four conjugated polymers used for conjugation length test.

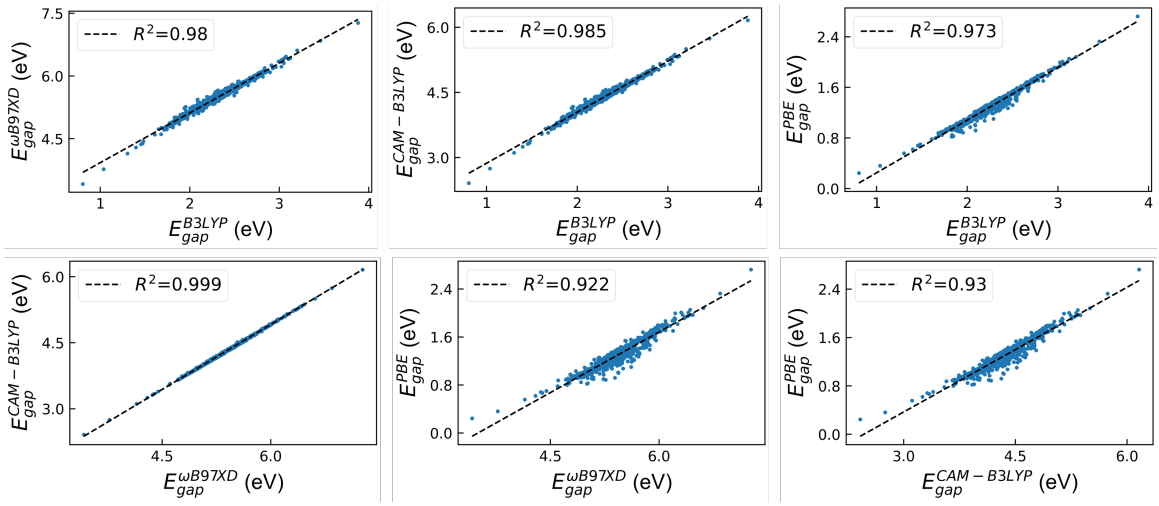

Figure S5: Linear fits of HOMO-LUMO gaps calculated with B3LYP, ωB97XD, CAM-B3LYP, and PBE exchange-correlation functionals.

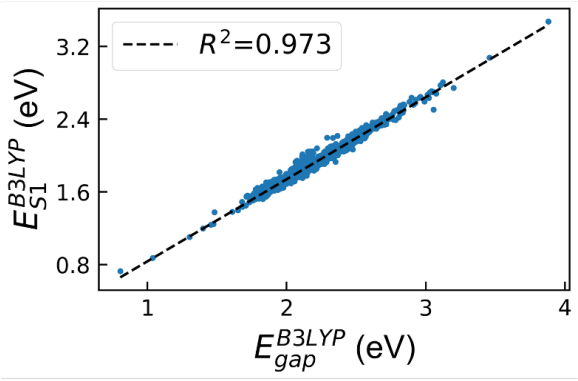

Figure S6: Correlation between HOMO-LUMO gap and lowest excited state (S1) calculated at the B3LYP level.

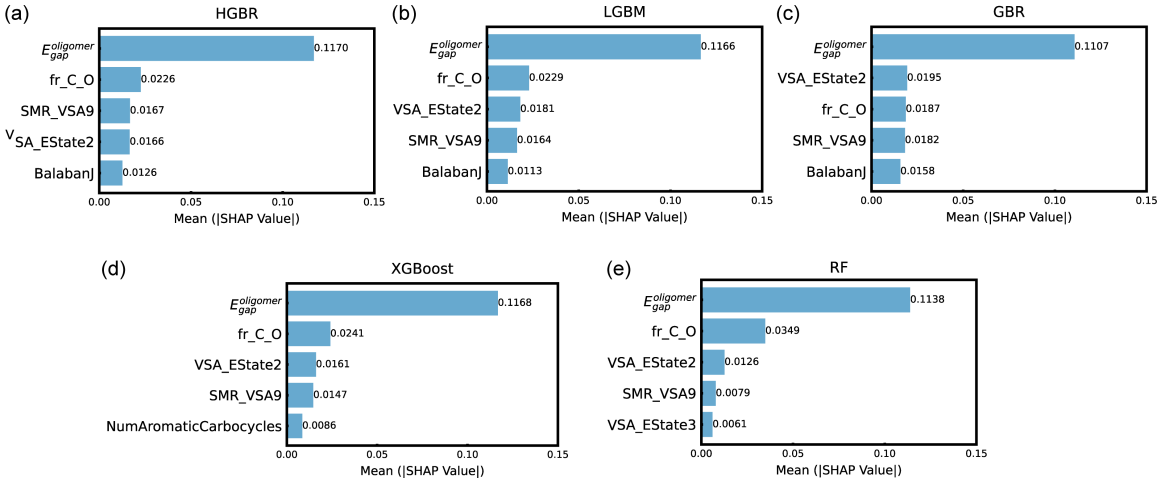

Figure S7: Mean absolute SHAP values of the top 5 features for predicting optical band gaps with (a) HGBM (b) LGBM (c) GBR (d) XGBoost (e) RF models. HOMO-LUMO gap was calculated from modified oligomer structures.

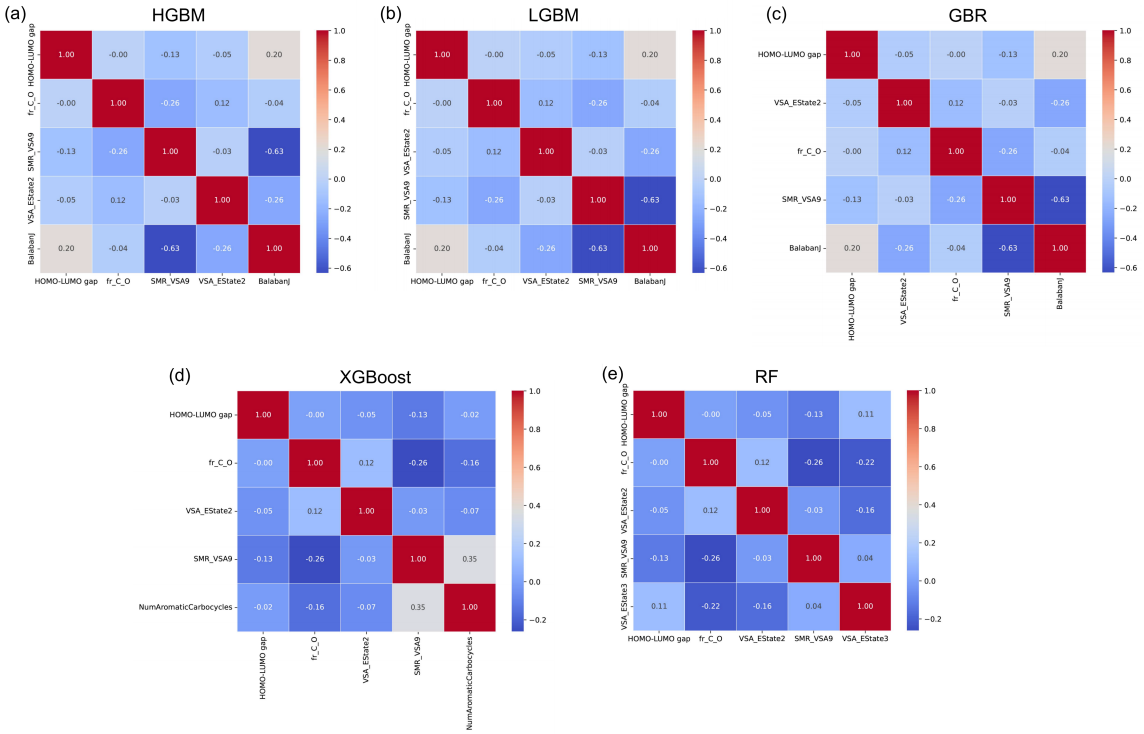

Figure S8: Pearson correlation coefficient map between the top 5 features for (a) HGBM (b) LGBM (c) GBR (d) XGBoost (e) RF models. HOMO-LUMO gap was calculated from modified oligomer structures.

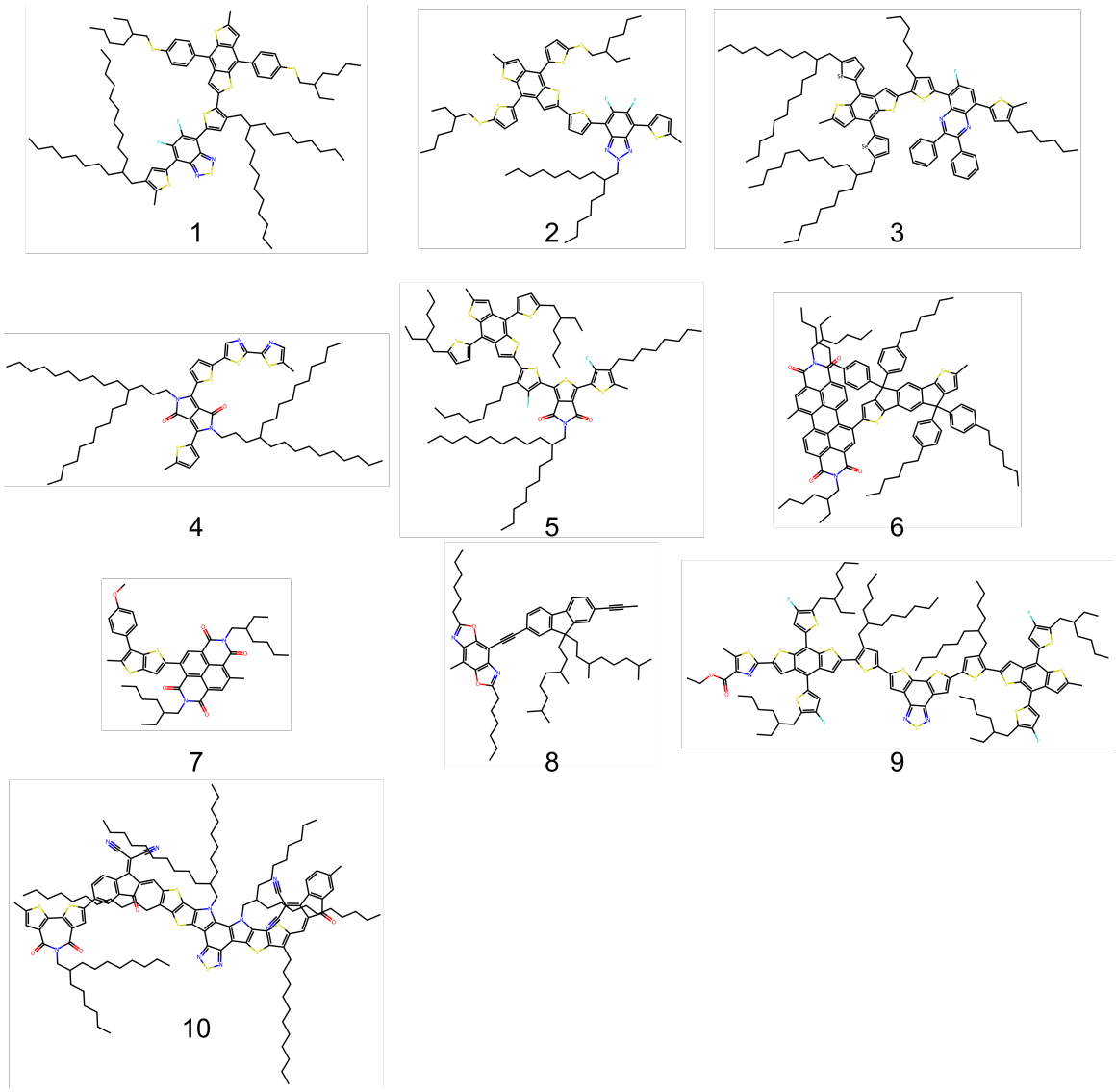

Figure S9: Chemical structures of 10 conjugated polymers.

Table S1: Statistical analysis of the experimentally measured HOMO, LUMO, and optical band gap (E_{gap}^{exp}) values of the conjugated polymers in the dataset with 1096 data points. Unit: eV.

Property	10%	90%	mean	std	max
HOMO	-5.6	-5.055	-5.334	0.225	-4.24
LUMO	-3.9	-3.31	-3.618	0.256	-2.59
E_{gap}^{exp}	1.465	1.98	1.716	0.206	2.39

Table S2: Feature selection from 209 RDKit descriptors for predicting optical band gaps of conjugated polymers and the performance metrics of XGBoost model trained with different combinations of pairwise Pearson correlation coefficient (P_{pair}) among descriptors and with respect to optical band gap (P_{gap}). The Bold indicates the optimal combination of P_{pair} and P_{gap} values. RMSE and MAE are measured in eV.

Round	P_{pair}	P_{gap}	# variables	RMSE	R^2	r	MAE
1	0.95	0.01	89	0.132	0.574	0.761	0.091
2	0.95	0.05	60	0.134	0.561	0.75	0.092
3	0.95	0.1	32	0.14	0.524	0.727	0.096
4	0.95	0.2	12	0.156	0.407	0.648	0.108
5	0.9	0.01	82	0.133	0.572	0.758	0.091
6	**0.9**	**0.05**	**54**	**0.134**	**0.565**	**0.753**	**0.092**
7	0.9	0.1	29	0.138	0.531	0.732	0.095
8	0.9	0.2	10	0.156	0.405	0.65	0.108

Table S3: The list of 54 RDKit descriptors for predicting experimental optical gap.

MaxAbsEStateIndex	PEOE_VSA1	SMR_VSA3	EState_VSA4
MinAbsEStateIndex	PEOE_VSA11	SMR_VSA4	EState_VSA5
MinEStateIndex	PEOE_VSA12	SMR_VSA6	EState_VSA10
NumAliphaticCarbocycles	PEOE_VSA13	SMR_VSA9	EState_VSA11
NumAliphaticHeterocycles	PEOE_VSA14	SMR_VSA10	fr_C_O
NumAliphaticRings	PEOE_VSA2	SlogP_VSA1	fr_aniline
NumAromaticCarbocycles	PEOE_VSA6	SlogP_VSA2	fr_bicyclic
NumAromaticHeterocycles	PEOE_VSA9	SlogP_VSA4	fr_halogen
NumHAcceptors	qed	SlogP_VSA10	fr_imide
VSA_EState2	MolWt	SlogP_VSA11	fr_oxazole
VSA_EState3	BalabanJ	SlogP_VSA12	fr_pyridine
VSA_EState8	TPSA	EState_VSA1	fr_ketone_Topliss
FractionCSP3	SMR_VSA1	EState_VSA2	
FpDensityMorgan1	SMR_VSA2	EState_VSA3	

Table S4: DFT calculated HOMO, LUMO, and gap (E_{gap}^{DFT}) of four conjugated polymers (CPs) with different repeating units. The chemical structures of these four CPs are shown in Figure S4. HOMO, LUMO, and E_{gap}^{DFT} are measured in eV.

Polymer	#repeating unit	#aromatic ring	#aromatic block	HOMO	LUMO	E_{gap}^{DFT}
Thiophene	1	1	1	-5.692	0.044	5.735
	2	2	2	-5.141	-1.066	4.075
	4	4	4	-4.789	-1.813	2.976
	6	6	6	-4.694	-2.112	2.582
	8	8	8	-4.639	-2.247	2.392
	10	10	10	-4.669	-2.289	2.38
BDT-T	1	4	2	-5.109	-1.465	3.644
	2	8	4	-4.946	-2.1	2.846
	3	12	6	-4.943	-2.252	2.691
ffQA-T	1	2	2	-5.598	-2.131	3.468
	2	4	4	-5.244	-2.486	2.758
	3	6	6	-5.126	-2.643	2.483
	4	8	8	-5.072	-2.727	2.346
	5	10	10	-5.043	-2.778	2.265
BDT-TT-QA-TT	1	8	4	-4.829	-2.355	2.474
	2	16	8	-4.717	-2.499	2.217

Table S5: Pearson correlation coefficients of HOMO-LUMO gap values calculated with B3LYP, ωB97XD, CAM-B3LYP, and PBEPBE exchange-correlation functionals. The modified oligomer structures were used for DFT single-point calculations.

B3LYP	1			
ωB97XD	0.99	1		
CAM-B3LYP	0.99	1	1	
PBEPBE	0.99	0.96	0.96	1
	B3LYP	ωB97XD	CAM-B3LYP	PBEPBE

Table S6: Performance metrics of linear regression between HOMO-LUMO gaps calculated with B3LYP, ωB97XD, CAM-B3LYP, and PBE exchange-correlation functionals, and experimental optical gaps.

xc functional	RMSE	R^2	r	MAE
B3LYP	0.144	0.512	0.716	0.111
ωB97XD	0.141	0.532	0.729	0.108
CAM- B3LYP	0.141	0.528	0.727	0.109
PBE	0.146	0.498	0.706	0.111

Table S7: Performance metrics of linear regression for predicting experimental optical gaps with HOMO-LUMO gaps (E_{gap}^{DFT}) and lowest excited state (S1) calculated at the B3LYP level.

Feature (eV)	RMSE	R^2	r	MAE
E_{gap}^{DFT}	0.144	0.512	0.716	0.111
S1	0.153	0.448	0.669	0.12

Table S8: The number of data points and the corresponding percentage of each group of conjugated polymers categorized based on donor and acceptor units, respectively.

	#Data point	ratio
All dataset	1096	100%
Donor units		
D1	512	46.70%
D2	107	9.80%
D3	75	6.80%
D4	73	6.70%
others	329	30%
Acceptor units		
A1	360	32.80%
A2	105	9.60%
A3	118	10.80%
A4	98	8.90%
others	415	37.90%

Table S9: The performance metrics of 6 Machine Learning models in predicting the experimental optical gaps of conjugated polymer, trained with RDKit descriptors combined with DFT-calculated HOMO-LUMO gaps. The best ML model is highlighted in bold. RMSE and MAE are measured in eV.

Input features	Model	RMSE	R^2	r	MAE
RDKit	HGBR	0.137	0.541	0.738	0.095
	LGBM	0.137	0.54	0.737	0.095
	GBR	0.145	0.49	0.709	0.105
	XGBoost	0.134	0.565	0.753	0.092
	AdaBoost	0.172	0.282	0.547	0.136
	RF	0.141	0.515	0.724	0.097
$E_{gap}^{monomer}$+RDKit	HBGR	0.123	0.632	0.798	0.086
	LGBM	0.124	0.632	0.798	0.086
	GBR	0.132	0.579	0.767	0.097
	XGBoost	0.124	0.632	0.798	0.086
	AdaBoost	0.157	0.406	0.645	0.121
	RF	0.13	0.595	0.778	0.09
$E_{gap}^{oligomer}$+RDKit	**HGBR**	**0.101**	**0.747**	**0.867**	**0.069**
	LGBM	0.101	0.747	0.868	0.069
	GBR	0.106	0.728	0.857	0.077
	XGBoost	0.104	0.738	0.861	0.07
	AdaBoost	0.129	0.599	0.781	0.1
	RF	0.107	0.723	0.853	0.074

Table S10: The performance metrics of 6 Machine Learning models in predicting the experimental optical gaps of conjugated polymer, trained with MACCS fingerprint combined with DFT-calculated HOMO-LUMO gaps. The best ML model is highlighted in bold. RMSE and MAE are measured in eV.

Input features	Model	RMSE	R^2	r	MAE
MACCS	HGBR	0.146	0.484	0.7	0.103
	LGBM	0.146	0.484	0.7	0.103
	GBR	0.145	0.489	0.705	0.105
	XGBoost	0.143	0.5	0.716	0.095
	AdaBoost	0.168	0.314	0.569	0.128
	RF	0.139	0.527	0.728	0.095
$E_{gap}^{monomer}$+MACCS	HBGR	0.135	0.565	0.756	0.097
	LGBM	0.134	0.567	0.757	0.097
	GBR	0.137	0.548	0.747	0.101
	XGBoost	0.132	0.578	0.766	0.094
	AdaBoost	0.16	0.384	0.63	0.124
	RF	0.13	0.592	0.774	0.093
$E_{gap}^{oligomer}$+MACCS	HGBR	0.111	0.699	0.839	0.078
	LGBM	0.111	0.697	0.839	0.079
	GBR	0.112	0.695	0.837	0.082
	XGBoost	0.113	0.69	0.836	0.078
	AdaBoost	0.136	0.551	0.748	0.108
	RF	**0.111**	**0.7**	**0.839**	**0.077**

Table S11: The performance metrics of 6 Machine Learning models in predicting the experimental optical gaps of conjugated polymer, trained with ECFP6 fingerprint combined with DFT-calculated HOMO-LUMO gaps. The best ML model is highlighted in bold. RMSE and MAE are measured in eV.

Input features	Model	RMSE	R^2	r	MAE
ECFP6	HGBR	0.116	0.673	0.823	0.08
	LGBM	0.116	0.673	0.823	0.08
	GBR	0.128	0.602	0.795	0.094
	XGBoost	0.111	0.701	0.84	0.075
	AdaBoost	0.16	0.381	0.641	0.123
	RF	0.12	0.649	0.815	0.082
$E_{gap}^{monomer}$+ECFP6	HBGR	0.11	0.706	0.844	0.075
	LGBM	0.11	0.706	0.844	0.075
	GBR	0.122	0.643	0.814	0.088
	XGBoost	0.108	0.718	0.85	0.074
	AdaBoost	0.149	0.463	0.693	0.114
	RF	0.119	0.661	0.821	0.082
$E_{gap}^{oligomer}$+ECFP6	HGBR	0.099	0.762	0.875	0.067
	LGBM	0.099	0.764	0.876	0.067
	GBR	0.104	0.74	0.864	0.076
	XGBoost	**0.097**	**0.773**	**0.881**	**0.065**
	AdaBoost	0.125	0.623	0.795	0.096
	RF	0.102	0.748	0.867	0.07

Table S12: Experimental optical gaps (E_{gap}^{exp}), predicted values (E_{gap}^{pred}) and the corresponding errors (RMASE and MAE) with XGBoost-2 and XGBoot-2-plus for 10 conjugated polymers. All the values are measured in eV.

	XGBoost-2		XGBoost-2-plus		Experiments	
index	E_{gap}^{pred}	error	E_{gap}^{pred}	error	E_{gap}^{exp}	Reference
1	1.935	-0.205	1.909	-0.179	1.73	Ref[5]
2	2.078	-0.188	1.966	-0.076	1.89	Ref[6]
3	1.669	-0.219	1.623	-0.173	1.45	Ref[7]
4	1.576	-0.266	1.496	-0.186	1.31	Ref[8]
5	1.708	0.192	1.751	0.149	1.9	Ref[9]
6	1.486	0.474	1.507	0.453	1.96	Ref[10]
7	1.649	0.371	1.644	0.376	2.02	Ref[11]
8	1.82	0.19	1.844	0.166	2.01	Ref[12]
9	2.064	0.696	2.642	0.118	2.76	Ref[13]
10	1.668	-0.287	1.464	-0.083	1.381	Ref[14]
RMSE		0.346		0.228		
MAE		0.309		0.196		

Table S13: The performance metrics for XGBoost model in predicting the experimental HOMO and LUMO levels of conjugated polymers with various molecular descriptors as input. RMSE and MAE are measured in eV.

Target	Model	Features	RMSE	R^2	r	MAE
HOMO	XGBoost-1-H	ECFP6	0.163	0.468	0.69	0.113
	XGBoost-2-H	$HOMO^{oligomer}$+ECFP6	0.158	0.503	0.716	0.109
LUMO	XGBoost-1-L	ECFP6	0.168	0.555	0.748	0.118
	XGBoost-2-L	$LUMO^{oligomer}$+ECFP6	0.161	0.595	0.775	0.112

Table S14: The default hyperparameters for six machine learning models.

Model	Hyperparameter	Default Value	Notes
HGBR (Histogram-Based Gradient Boosting Regressor)	max_iter	100	Number of boosting iterations.
	max_depth	None	No limit on tree depth.
	learning_rate	0.1	Weighting of each boosting step.
LGBMRegressor	max_iter	default	Automatically determined.
	max_depth	-1	Unlimited depth (-1 indicates no limit).
	learning_rate	0.1	Weighting of each boosting step.
GBR (Gradient Boosting Regressor)	max_iter	default	Automatically determined.
	max_depth	3	Maximum depth of each tree.
	learning_rate	0.1	Weighting of each boosting step.
XGBRegressor (XGB)	max_iter	default	Automatically determined.
	max_depth	6	Maximum depth of each tree.
	learning_rate	0.3	Weighting of each boosting step.
RandomForestRegressor (RF)	max_iter	default	Automatically determined.
	max_depth	None	No limit on tree depth.
AdaBoostRegressor	max_iter	default	Automatically determined.
	learning_rate	1.0	Weighting of each boosting step.

References

1. Kyaw Zin PP, Borrel A, and Fourches D. Benchmarking 2D/3D/MD-QSAR models for Imatinib derivatives: how far can we predict? Journal of Chemical Information and Modeling 2020;60:3342–60.
2. Sohlberg K and Foster ME. What's the gap? A possible strategy for advancing theory, and an appeal for experimental structure data to drive that advance. RSC advances 2020;10:36887–96.
3. Sun H and Autschbach J. Electronic energy gaps for π-conjugated oligomers and polymers calculated with density functional theory. Journal of Chemical Theory and Computation 2014;10:1035–47.
4. Salzner U and Aydin A. Improved prediction of properties of π-conjugated oligomers with range-separated hybrid density functionals. Journal of chemical theory and computation 2011;7:2568–83.
5. Du Z, Cai M, Du L, et al. Effect of alkylthiolated hetero-aromatic rings on the photovoltaic performance of benzodithiophene-based polymer/fullerene solar cells. Synthetic Metals 2021;276:116756.
6. Zhai X, Wang X, Zhu K, et al. Random terpolymers for high-performance semitransparent polymer solar cells. Dyes and Pigments 2021;195:109680.
7. Caliskan M, Erer MC, Aslan ST, Udum YA, Toppare L, and Cirpan A. Narrow band gap benzodithiophene and quinoxaline bearing conjugated polymers for organic photovoltaic applications. Dyes and Pigments 2020;180:108479.
8. Ren S, Zhang W, Wang Z, Yassar A, Liao Z, and Yi Z. Synergistic Use of All-Acceptor Strategies for the Preparation of an Organic Semiconductor and the Realization of High Electron Transport Properties in Organic Field-Effect Transistors. Polymers 2023;15:3392.
9. Kim J, Lee WH, Park JB, Hwang DH, and Kang IN. Synthesis and characterization of the fluorinated thieno [3, 4-c] pyrrole-4, 6-dione-based donor-acceptor polymers for organic solar cells. Dyes and Pigments 2019;160:403–9.
10. Zhao X, Wen Y, Ren L, Ma L, Liu Y, and Zhan X. An acceptor-acceptor conjugated copolymer based on perylene diimide for high mobility n-channel transistor in air. Journal of Polymer Science Part A: Polymer Chemistry 2012;50:4266–71.
11. Gunturkun D, Isci R, Faraji S, Sütay B, Majewski LA, and Ozturk T. Synthesis and characterization of naphthalenediimide-thienothiophene-conjugated polymers for OFET and OPT applications. Journal of Materials Chemistry C 2023;11:13129–41.
12. Liao Z, Hu D, Tang H, et al. 18.42% efficiency polymer solar cells enabled by terpolymer donors with optimal miscibility and energy levels. Journal of Materials Chemistry A 2022;10:7878–87.
13. Intemann JJ, Hellerich ES, Tlach BC, et al. Altering the conjugation pathway for improved performance of benzobisoxazole-based polymer guest emitters in polymer light-emitting diodes. Macromolecules 2012;45:6888–97.

14. Sun H, Liu B, Ma Y, et al. Regioregular narrow-bandgap n-type polymers with high electron mobility enabling highly efficient all-polymer solar cells. Advanced Materials 2021;33:2102635.